Author(s): Lindgren, Johan; Olbert-Majkut, Adriana; Pettersson, Mika; Kiljunen, Toni

Title: Raman spectroscopy and crystal-field split rotational states of photoproducts CO and H2 after dissociation of formaldehyde in solid argon

Year: 2012

Version:

Please cite the original version:

Lindgren, J., Olbert-Majkut, A., Pettersson, M., & Kiljunen, T. (2012). Raman spectroscopy and crystal-field split rotational states of photoproducts CO and H2 after dissociation of formaldehyde in solid argon. The Journal of Chemical Physics, 137(16), 164310-11. https://doi.org/10.1063/1.4762866

Raman spectroscopy and crystal-field split rotational states of photoproducts CO and H2 after dissociation of formaldehyde in solid argon

Johan Lindgren, Adriana Olbert-Majkut, Mika Pettersson, and Toni Kiljunen

Citation: The Journal of Chemical Physics **137**, 164310 (2012); doi: 10.1063/1.4762866
View online: http://dx.doi.org/10.1063/1.4762866
View Table of Contents: http://scitation.aip.org/content/aip/journal/jcp/137/16?ver=pdfcov
Published by the AIP Publishing

Raman spectroscopy and crystal-field split rotational states of photoproducts CO and H_2 after dissociation of formaldehyde in solid argon

Johan Lindgren,[1,a)] Adriana Olbert-Majkut,[2] Mika Pettersson,[1] and Toni Kiljunen[1]
[1]*Department of Chemistry, Nanoscience Center, P.O. Box 35, FI-40014 University of Jyväskylä, Finland*
[2]*Faculty of Chemistry, Wroclaw University, F. Joliot-Curie 14, 50-383 Wroclaw, Poland*

(Received 13 July 2012; accepted 9 October 2012; published online 26 October 2012)

Raman signal is monitored after 248 nm photodissociation of formaldehyde in solid Ar at temperatures of 9–30 K. Rotational transitions $J = 2 \leftarrow 0$ for para-H_2 fragments and $J = 3 \leftarrow 1$ for ortho-H_2 are observed as sharp peaks at 347.2 cm^{-1} and 578.3 cm^{-1}, respectively, which both are accompanied by a broader shoulder band that shows a split structure. The rovibrational spectrum of CO fragments has transitions at 2136.5 cm^{-1}, 2138.3 cm^{-1}, 2139.9 cm^{-1}, and 2149 cm^{-1}. To explain the observations, we performed adiabatic rotational potential calculations to simulate the Raman spectrum. The simulations indicate that the splitting of rotational transitions is a site effect, where H_2 molecules can reside in a substitution site, in addition to an interstitial site. In the former site, rotational motion is unperturbed by the electrostatic field of the host atoms, while the latter site splits the excited rotational manifolds, $J = 2$ and 3, into doublet and triplet structures, respectively. For CO, the spectrum can be ascribed to monomeric species in single- and double-substitution sites, to a dimeric species $(CO)_2$, and to a CO–H_2O complex. The simulations show that a nearest-neighbor molecular complex CO–H_2 is not responsible for any of the observed spectral fingerprints. The cause of the exit of the molecular hydrogen from the initial cage can be traced to high translational energy of the fragment after the photodissociation. After the matrix has reached a thermal equilibrium, a diffusion driven formation of the complex is possibly hindered by the high rotational zero-point energy developed upon complexation. © *2012 American Institute of Physics*. [http://dx.doi.org/10.1063/1.4762866]

I. INTRODUCTION

Photodissociation of molecules in a condensed phase, like in rare gas matrices, leaves the photoproducts with excess energy which is distributed among their degrees of freedom inside a cage restricting the motion of the fragments. The surroundings can have a large impact on the fate of the species, thus insight into the dynamics in the condensed phase can be achieved by probing the photoproducts. After the photodissociation, there is a possibility that the fragments undergo a geminate recombination, or that a fragment escapes the cage. The cage exit can happen either directly if there is enough momentum to climb over the potential barrier (created by the host atoms) or indirectly after cage deformations. Both exit and recombination mechanisms have been observed previously with hydrogen halides[1,2] in solid argon. In addition to the excess energy, the probability can be affected by controlling the vibrational and rotational initial state distributions.[3,4] Perhaps a more exotic outcome is the formation of stable compounds between rare gas atom and photofragments.[5] In argon, such was found after photodissociation of HF, resulting in the first stable argon compound HArF.[6] Migration can also occur after annealing the sample, leading to a thermally induced cage exit, without any requirement of photon excitation.[7]

Formaldehyde (FA) has been the workhorse in the field of photodynamics for its being the prototype of more complex reactions in the gas phase while remaining as a tractable problem. See Ref. 8 for an extensive collection of experimental and numerical studies on the dynamics in gas phase. Two dissociation pathways arise for FA,

$$H_2CO + h\nu \rightarrow H_2 + CO, \quad (1)$$

$$H_2CO + h\nu \rightarrow H + HCO\,, \quad (2)$$

where pathway (1) is commonly referred as the molecular dissociation, and (2) as the radical dissociation. In pathway (2), HCO could further dissociate to a hydrogen atom and a molecular CO. In 2004, a new mechanism for pathway (1) was found, named as "roaming" mechanism due to high mobility of one hydrogen atom before snatching the remaining hydrogen atom from HCO.[9] Although the end products are the same as in molecular dissociation the roaming is best described as a "frustrated radical dissociation."[10]

The decomposition of FA is initiated by the $\tilde{A}\ ^1A_2(S_1) \leftarrow \tilde{X}\ ^1A_1(S_0)$ absorption in the UV. After the absorption, excess energy on the first excited singlet state S_1 is distributed among the vibrational modes of FA. In a solid environment, some of the vibrational energy is lost to the surrounding cage atoms in collisions. The exact details of the collision dynamics eventually dictate the dissociation outcome. The processes that can lead to dissociation are internal conversion (IC) to S_0 and intersystem crossing (ISC) to T_1 from where ISC to S_0 can also occur. The molecular products are formed exclusively on S_0, whereas the radical products can be formed on both T_1 and S_0.[8] Dissociation occurs if the amount of

a)Electronic mail: johan.lindgren@jyu.fi.

vibrational energy available after the IC and/or ISC is larger than the energy required for bond breaking.

In the gas phase, the branching ratio between the above reaction pathways (channels) is known to depend on the excitation energy. As the photolysis energy increases over 30 000 cm^{-1}, the radical pathway becomes dominant, and at these energies also the roaming mechanism comes into effect. Characteristic for the molecular pathway (direct dissociation) is that the excess energy after dissociation is mostly (65%) distributed to translational energy of H_2. The roaming mechanism, on the other hand, leads to vibrationally highly excited molecular hydrogen while the distributed translational energy is much lower than in the direct dissociation case.[9] Regarding the radical channel, the portion of energy that goes to translation is diminished even further.[11–15]

In the solid phase, Vaskonen and Kunttu[16] used EPR and IR spectroscopies to study the pathways (1) and (2). Their conclusion from EPR studies was that compared to heavier rare gases, in argon, the hydrogen atoms are least abundant after the dissociation and that they occupy substitution sites. They noted, however, that the temperature (16 K) in their EPR measurement was near the onset of diffusion of hydrogen atoms from interstitial sites. Their IR spectrum in the region of vibrational transition of CO showed a peak at 2138 cm^{-1} after photolysis that split into three peaks after annealing at 30 K, and were assigned to a CO–N_2 complex, a CO monomer, and a $(CO)_2$ dimer. They did not identify any new absorption feature that would belong to the CO–H_2 complex. Prior studies[17–19] of FA in argon have shown a similar peak at 2138 cm^{-1} after dissociation but no annealing studies were made.

Raman spectroscopy, being complementary to IR spectroscopy (and EPR as well), can give further understanding of the reaction pathways, and it has been used in our group to identify the photoproducts and their complexes after photodissociation of formic acid in solid argon.[20] The same authors also used Raman to study vibrational motion of acetic acid[21] and formic acid[22] in monomeric and dimeric forms in solid argon. In the gas phase, Raman spectroscopy has been used to probe the H_2 photoproduct[23,24] but to our best knowledge, there is no condensed phase study of photodissociation of formaldehyde that has used Raman for probing the photoproducts. Therefore, our present study provides additional information on the dynamical properties and the local structure of the system, and gives further insight into the reaction mechanism.

Our measured Raman spectra show a sharp central peak which is expected for a rotational excitation but in addition a shoulder on both sides of the sharp peak is observed. This indicates a crystal-field effect on the rotational motion, and we have simulated this by constructing the rotational potential for H_2 in argon lattice. This is first done without CO as if the molecules were isolated completely from each other in the matrix, and then with CO in the same cubic unit cell. The measured fundamental vibrational frequency region of CO has the same spectral feature as seen before in the isolated case, i.e., when only gaseous CO is co-deposited with argon.[25] However, due to the observed band structure in the rotational spectrum of hydrogen, we have simulated the rotational motion of CO to see the possible effect of a nearby hydrogen molecule.

II. METHODS

A. Experimental methods

Formaldehyde was released from paraformaldehyde (purity >95 %, Fluka) and mixed with argon (purity 99.999%, Messer) in a vacuum line and stored in a 5 L pyrex bulb prior to the matrix deposition. Dilution ratios were set to 1:150 and 1:750 using standard manometric techniques. Formaldehyde was purified by several freezing–annealing cycles in a high-vacuum system. Argon was used without additional purification.

The gas mixture was deposited at 19 K onto a thin (150 μm) sapphire substrate kept at the deposition temperature in a closed-cycle cryostat (APD Cryogenics) equipped with quartz outer windows. The deposition rate was kept at 0.11 mmol/min and the total amount of deposited gas was 12–40 mmol. The thickness of the samples was ca. 40 μm. Lakeshore 330 temperature controller equipped with a silicon diode was used for controlling the temperature of the samples.

Deposited FA/Ar mixture was cooled to 9 K and photolyzed with an excimer laser (Lambda Physik Optex) operating at 248 nm (KrF) with pulse intensity of ca. 13 mJ cm^{-2} and pulse repetition rate of 10 Hz at the sample. The beam area of the excitation laser was ca. 0.35 cm^2. To dissociate the FA, 15 000 and 10 000 pulses were used, and the estimated photon fluxes I were 2.4×10^{20} and 1.6×10^{20} photons/cm^2 at guest/host ratios 1/750 and 1/150, respectively. Raman signal was recorded after the dissociation at 9 K and at 30 K, 20 K, and 10 K in that order, using previously described setup.[20,25] The Raman and excimer laser beams were adjusted so that the measured signal originated from the photolyzed volume. By observing the intensity change of a peak at ca. 1744 cm^{-1} belonging to the $\nu(C=O)$ stretching vibration in FA, we estimate that at least 60% of the FA molecules were dissociated. Dissociation cross section σ_{cross} can be calculated from $\ln(N/N_0) = -I\sigma_{cross}$, where the ratio N/N_0 is the number of dissociated molecules per initial number of molecules. Above numbers give an estimate of 2.1×10^{-21} and 3.2×10^{-21} cm^2 for the dissociation cross sections at 1/750 and 1/150 dilution ratios, respectively. These are comparable to cross sections obtained in Ref. 16.

B. Theoretical methods

Rotational motion of isolated carbon monoxide in solid argon was considered in our previous paper[25] where we optimized the lattice structure for each orientation of the molecule with respect to crystal axes, referred as adiabatic method. Now we employ the same method with modifications when we simulate the rotational potential of isolated hydrogen and find out which effect the adding of CO in the first or second coordination shell makes to the potential. This is also done *vice versa*, studying the effect of hydrogen on the spectrum of carbon monoxide.

TABLE I. The trapping coordinates for hydrogen molecule site labels S1, S2, S3, and O in solid argon. For the H_2–CO complexes studied, the CO resides at monosubstitution site at origin. Lattice constant a is 5.31 Å.

S1	S2	S3	O
$(\frac{a}{2}, \frac{a}{2}, 0)$	(a, 0, 0)	(a, 0, a)	$(\frac{a}{2}, \frac{a}{2}, \frac{a}{2})$

Our simulation box included 256 argon atoms, forming a fcc lattice with lattice constant $a = 5.31$ Å. Periodic boundary conditions were implemented to remove the undesired surface effects due to the limited number of argon atoms. In the case, where the photoproduct CO–H_2 complex is considered, we assume that the precursor, for steric reasons, occupies a double-substitution (DS) site. CO molecule was put in a substitution site at origin, and H_2 at four different nearby sites. These include three substitution sites and one interstitial site with labeling S1, S2, S3, and O, respectively. Details regarding the different trapping geometries can be found in Table I.

The 248 nm excitation energy puts the molecule in the excited electronic state S_1 with approximately 12 000 cm^{-1} of vibrational energy.[26,27] At this energy, the radical channel is the dominant pathway for dissociation over the two molecular channels, the direct and the roaming. In fact, Vaskonen and Kunttu[16] saw a signal from the hydrogen atom in substitution and interstitial sites with similar matrix conditions as in the present case but after more intense irradiation. The cage effect would decrease the probability of the cage exit of the H atom as the translational energy of atomic hydrogen is substantially smaller than that of the molecular hydrogen after a dissociation via the molecular pathway. The conversion of H+HCO to H_2+CO via a mechanism similar to roaming but without the long range of the C–H bong elongation is also one possible outcome. However, the exact details of the cage effect on the dissociation dynamics are unknown. The abstraction of hydrogen from HCO radical could lead to CO–H_2 complex formation at the initial site, but if we take the direct molecular pathway as the dissociation channel, the initial kinetic energy induces a ballistic trajectory for the molecular hydrogen which is expected to lead to a cage exit.

The van der Waals complex CO–H_2 has been recently observed, and the IR spectra for both para- and orthohydrogen spin isomers were assigned by theoretical means.[28] For consistency, we also consider a formation of a nearest-neighbor intermolecular complex CO–H_2, where the hydrogen is located in the initial vacancy nearest to CO. This situation is referred as S1 and the molecular photoproducts are nearest-neighbors with initial distance $a/\sqrt{2}$. S2 has H_2 at a lattice constant away from CO, and S3 is the furthest trapping site considered, where an argon atom has entered between the fragments. At site O, hydrogen is separated from CO by a triangular "window" formed from three Ar atoms nearest-neighbor to CO. If CO is left out from the simulation box, the substitution sites S1, S2, and S3 give an identical signal and only one of these sites needs to be considered (in addition to the interstitial site).

1. Rotational Raman spectrum of H_2

a. Potential energy surfaces In our previous studies of carbon monoxide, due to slow rotation, the surrounding lattice atoms were expected to be able to follow the reorientation of molecular axis. This leads to adiabatic surfaces for rotation where host atoms and the center of mass of the guest molecule relax to their equilibrium positions. This adiabatic assumption breaks down with hydrogen, making the concept of synchronously moving host atoms with reorientation of the molecule invalid. Instead the molecular rotation is decoupled (almost) entirely from the surrounding lattice. We do not imply that the resulting lattice configuration is unaffected by the molecule but rather consider a case where the host atoms feel a presence of spherically symmetric species. This is achieved by using only the isotropic part of the interaction potential in our relaxation procedure which is done only at the beginning of the simulation to obtain a time-averaged cage interaction.

The space-fixed frame coincides with the crystal frame, and the molecular orientation is expressed in angular variables θ, ϕ of the spherical coordinate system. Rotational potential $V_I(\theta, \phi)$ for isolated (I) H_2 is obtained as a pairwise sum of interaction potentials

$$V_I(\theta, \phi) = \sum_{i<j} V_{\mathrm{Ar_i,Ar_j}} + \sum_i V_{\mathrm{Ar_i,H_2}}(\xi, R, \Theta)\,. \qquad (3)$$

The interatomic potential Ar–Ar[29] is a function of distance between rare gas atoms with the well depth -100 cm^{-1} at equilibrium distance $R_{\min} = 3.75$ Å. We use a three-dimensional Ar–H_2 interaction potential based on the exchange-Coulomb model with five empirically determined parameters.[30] Jacobi coordinates $\vec{r} = r\hat{r}$, $\vec{R} = R\hat{R}$, and $\Theta = \cos^{-1}(\hat{r} \cdot \hat{R})$ were used. Vector $\vec{r}$ points from atom to atom in hydrogen, with r as the bond length, $\vec{R}$ points from molecular center of mass to each rare gas atom Ar_i. Collinear geometry H–H–Ar is obtained when $\Theta = 0$. The variable ξ is defined as $\xi = (r - r_0)/r_0$, where $r_0 = 1.448739a_0$ is fixed to the expectation value of molecular bond length in the ground rovibrational state. The H_2–Ar intermolecular potential is plotted in Panel (a) of Fig. 1. The potential energy surface is expanded as a power series in vibrational stretching coordinate[30]

$$V_{\mathrm{Ar_i,H_2}}(\xi, R, \Theta) = \sum_{k=0}^{4} \langle \xi^k \rangle U_k(R, \Theta)\,, \qquad (4)$$

where $k = 0$ is the isotropic part of the interaction (well depth -51 cm^{-1} at $R_{\min} = 3.6$ Å). The $\langle \xi^k \rangle$ is the matrix element $\langle \nu', j' | \xi^k | \nu'', j'' \rangle$.[31] We do not explicitly need the bond length r in our relaxation or rotational potential simulations but instead use the expectation values $\langle 00 | \xi^k | 00 \rangle$ for para-H_2 (pH_2) and $\langle 01 | \xi^k | 01 \rangle$ for ortho-H_2 (oH_2).

When CO is added in the lattice, CO–H_2 pair-potential must be taken into consideration (in addition to CO–Ar), and now the rotational potential is

$$V_P(\theta, \phi) = V_I(\theta, \phi) + \sum_i V_{\mathrm{Ar_i,CO}}(r_{\mathrm{CO}}, \tilde{R}, \tilde{\Theta}) + V_{\mathrm{H_2\text{-}CO}}(R_{\mathrm{mol}}, \Theta_1, \Theta_2, \Phi)\,. \qquad (5)$$

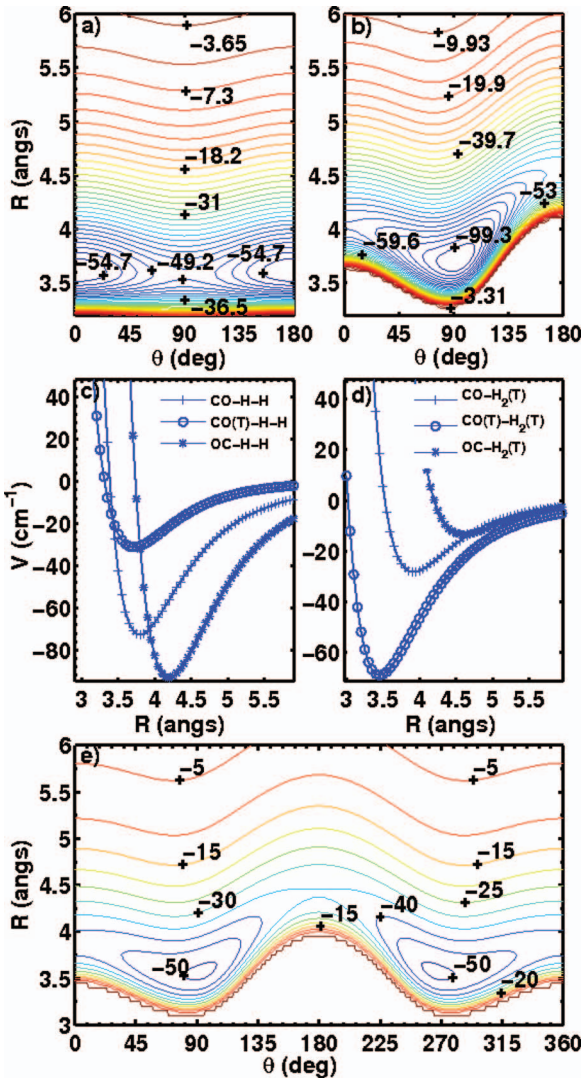

FIG. 1. Most of the pair-potentials (in cm^{-1}) used in this work. (a) H_2–Ar pair-potential. Global minimum corresponds to linear configuration H–H–Ar. (b) The CO–Ar intermolecular potential. The minimum energy configuration is a near T-shape with argon slightly closer to oxygen end. The CO bond length r_{CO} was 1.1324 Å. (c) CO–H_2 pair-potential, collinear configuration where either the oxygen (CO–H–H), or the carbon (OC–H–H) end points to hydrogen, and T-shape where the CO molecular axis is perpendicular to H_2 molecular axis (open circles). (d) CO–H_2 pair-potential, perpendicular configuration. In (c) and (d), the dihedral angle was set to zero. (e) CO–H_2 potential, where hydrogen molecule is considered as a spherical species, exhibits a T-shaped global minimum.

Jankowski and Szalewicz[32] obtained the four-dimensional potential surface for CO–H_2 complex within supermolecular approach using the coupled-cluster method CCSD(T). They described the configuration of the complex with Jacobian coordinates $\vec{r}_1$, $\vec{r}_2$, $\vec{R}$, $\Theta_1 = \cos^{-1}(\hat{r}_1 \cdot \hat{R})$, $\Theta_2 = \cos^{-1}(\hat{r}_2 \cdot \hat{R})$, and $\Phi = \hat{n}_{r_1,R} \cdot \hat{n}_{r_2,R}$. The variables r_i ($i = 1$ for H_2) describe the vibrational stretching coordinate, R is the distance between the center of masses of the molecules, angles Θ_i describe the orientation of molecular axes with respect to $\vec{R}$, and Φ is the dihedral angle. Orientation $\Theta_1 = \Theta_2 = 0$ corresponds to collinear geometry C–O–H–H, and $\Theta_1 = 0$, $\Theta_2 = 180$ to O–C–H–H geometry. These are the preferred geometries, the latter being the global minimum. In the construction of the intermolecular potential surface, the bond length of CO is set to $r_{CO} = 1.1324$ Å, matching with the C–O distance averaged over the ground vibrational state. The final 4D intermolecular CO–H_2 surface was obtained by averaging the vibrational motion of H_2. In the relaxation part of the simulation, the interaction between CO and H_2 in the complex was averaged so that the hydrogen molecule has only isotropic contribution to the pair-potential. The four-dimensional intermolecular potential at different geometries is plotted in Panels (c) and (d) of Fig. 1 and the isotropic potential is shown in Panel (e). The CO–Ar potential[33] (Panel (b) of Fig. 1) is the same as used before in our study[25] for isolated CO, with the bond length fixed to $r_{CO} = 1.1324$ Å in the potential simulation.

b. Rotational states With the potential energy surfaces $V(\theta, \phi)$ for rotation at hand, the rotational states are obtained by diagonalization of the Hamiltonian matrix

$$H_{jm,j'm'} = \Big[B_0^{(CO/H_2)} j(j+1) \underbrace{- D_0 j^2 (j+1)^2}_{\text{Centrifugal term only for } H_2}\Big]\delta_{jj'}\delta_{mm'} + \int d\Omega\, Y^*_{jm}(\theta,\phi) V_{P/I}(\theta,\phi) Y_{j'm'}(\theta,\phi) \quad (6)$$

in real-valued spherical harmonic basis. The evaluations were done on a coarse grid with a 5° spacing, and then spline-interpolated to final $[\theta, \phi]$ grid size of 180×360 points. The pseudorotating cage model[34] cannot be used here to gain estimation of the rotational constant, so we use the experimental results to scale the rotational constant $B_0^{(H_2)}$ and also the distortion constant D_0 in the centrifugal term (only for H_2). The intensity for each transition is the absolute square of the transition matrix element of induced Hamiltonian operator in rotational space averaged over crystal orientations with respect to the laboratory frame[25]

$$I_{i\to f} = \frac{16\pi\,\Delta\alpha^2\epsilon^4}{15^2} \sum_{m=-2}^{2} |\langle \Psi_i | Y_{2m}(\theta,\phi) | \Psi_f \rangle|^2 , \quad (7)$$

where ϵ is the electric field strength, and $\Delta\alpha = \alpha_{||} - \alpha_{\perp}$ is the anisotropy of polarizability tensor, both fixed to unity. Calculated frequencies are convoluted by a Lorentzian with FWHM = 1 cm^{-1} for the visualization of the simulated spectra.

To properly simulate the rotation of H_2, we have to pick certain orientations of CO with respect to crystal frame. The orientations that were chosen correspond to minima in the adiabatic potential of CO. The final Raman spectrum S of H_2 is then a sum of signals S_i originating from different orientations $(\theta^{(i)}_{min}, \phi^{(i)}_{min})$ of molecular axis of CO, and we use the ground state wavefunction Ψ_{CO} of CO to weight the different signals:

$$S = \sum_i \left|\Psi_{CO}\left(\theta^{(i)}_{min}, \phi^{(i)}_{min}\right)\right|^2 S_i \, . \quad (8)$$

2. Rovibrational Raman spectrum of CO

After the dissociation, the orientation of CO is assumed to be such that the carbon end is pointing toward the hydrogen. We will concentrate on a situation where the hydrogen leaves this site, and argon atom fills the vacancy. The adiabatic

method is modified to include a hydrogen molecule in the lattice. Assuming pairwise additivity of the different interaction potentials, we relax the structure with every CO orientation and the resulting potential is a sum of different interactions calculated from relaxed configuration. Now we take only the isotropic part of H_2–X interactions in the total adiabatic rotational potential

$$V_P^{(\mathrm{sph})}(\theta,\phi) = \sum_{i<j} V_{\mathrm{Ar_i,Ar_j}} + \sum_i V_{\mathrm{Ar_i,CO}}(r_{\mathrm{CO}}, \tilde{R}, \tilde{\Theta}) + \sum_i V^{(\mathrm{sph})}_{\mathrm{Ar_i,H_2}}(R) + V^{(\mathrm{sph})}_{\mathrm{H_2-CO}}(R_{\mathrm{mol}}, \Theta_2)\,. \quad (9)$$

The resulting potential was then inserted into Schrödinger equation (SE) and the computed eigenvectors and eigenenergies were used to simulate the rovibrational Raman spectrum. The pseudorotating cage model is not proper here due to broken symmetry of the cage caused by nearby hydrogen molecule so the rotational constant $B_0^{(\mathrm{CO})}$ was fixed to the gas-phase value 1.92 cm^{-1}. Here we do not consider the centrifugal term.

The $v = 0 \rightarrow 1$ fundamental frequency (band origin) was calculated using the 3D potential energy surface of CO–Ar pair-potential in Eq. (5), now with r_{CO} as a variable, summing over a sufficient number of nearest argon atoms, and solving for the vibrational states by a Fourier-Grid-Hamiltonian method[35] on a grid with 256 points.

III. RESULTS

A. Raman measurements

Rotational Raman spectra for $p\mathrm{H_2}$ and $o\mathrm{H_2}$ are shown in Fig. 2. At the two dilutions 1/750 (bottom) and 1/150 (top), a sharp central peak dominates the spectra, whereas the underlying broad band is temperature dependent and contains a split sub-structure. In particular, for $p\mathrm{H_2}$, the sharp peak is resolved at 347.2 cm^{-1} in all the spectra. When the 1/750 sample is annealed after the dissociation at 9 K, two peaks resolve from the broad band at 344.8 cm^{-1} and 350.5 cm^{-1}. For the less diluted 1/150 sample, the broad band remains unresolved. Only at the 30 K temperature, a shoulder peak is seen on the blue side of the main peak. In the case of $o\mathrm{H_2}$, the sharp main peak is visible at 578.3 cm^{-1} in all the spectra. Here, the splitting is more profound and a stable band is clearly resolved at 572.1 cm^{-1}. The blue side of the main peak is broader, and only after annealing the peak at 583.6 cm^{-1} is resolved. At the 1/150 concentration, similar to the $p\mathrm{H_2}$ region, a shoulder appears on the blue side at 580.4 cm^{-1} after annealing. The appearance of the sharp peaks after the annealing, as compared to the broad, rather structureless spectra right after the photodissociation at 9 K, can be explained by lattice relaxation. Overall, a sharp central peak along with side bands is observed regardless of the dilution ratio or the spin isomer.

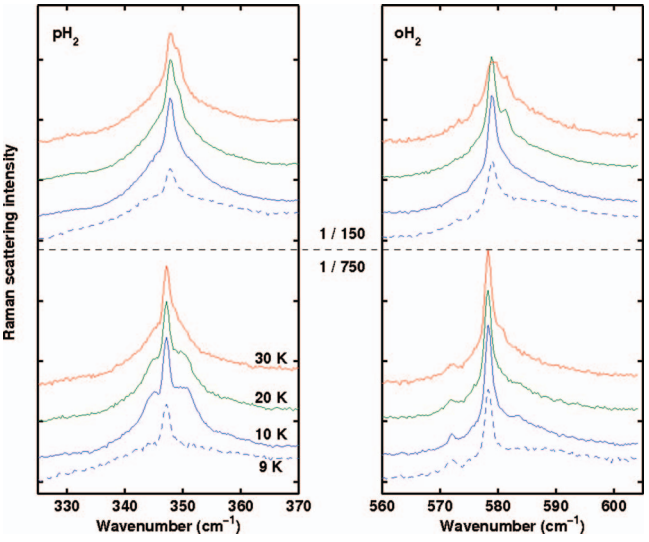

FIG. 2. Rotational Raman spectra for the two matrix-isolated hydrogen species at precursor dilution ratios 1/750 (bottom) and 1/150 (top). Dissociation of formaldehyde is induced at 9 K and the sample is then probed (broken line). Subsequent measurements were then performed at 30 K, 20 K, and 10 K in that order. Raman shifts correspond to $J = 2 \leftarrow 0$ and $J = 3 \leftarrow 1$ rotational excitations for $p\mathrm{H_2}$ and $o\mathrm{H_2}$, respectively. The spectral features are identified as a stable central peak and a temperature dependent broad band structure.

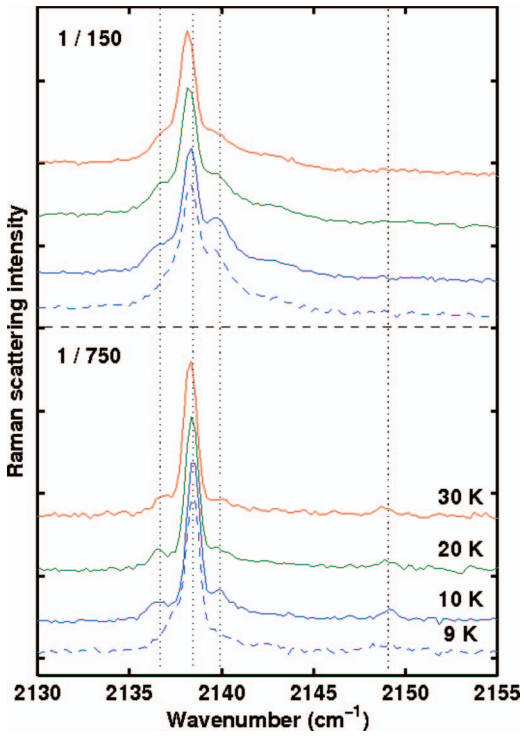

FIG. 3. Measured Raman signals in the fundamental frequency region of CO for dilution ratios 1/150 (upper) and 1/750 (lower). The sample conditions are the same as for H_2 in Fig. 2. The spectra exhibit a structure (indicated by the dotted lines) due to two trapping sites and a complex formation analyzed before for a pure CO/Ar sample.[25]

The experimental results for CO stretching region are shown in Fig. 3. In the more diluted sample (FA/Ar = 1/750), immediately after the photodissociation at 9 K, sharp peak is observed at 2138.3 cm^{-1}. After annealing the sample at 30 K, bands emerge at 2136.5 cm^{-1}, 2139.9 cm^{-1}, and 2149 cm^{-1}. The peak positions match with our previously measured bands for the isolated CO in Ar, where we referred to these peaks as A, B, C, and D.[25] We can now invoke the same assignment here. Peak A belongs to librating CO in a DS site with carbon

end pointing toward the empty site. Peak B on the other hand belongs to CO in a single-substitution (SS) site with rotational motion best described as hindered rotation. Peak C, hereafter referred as the dimer peak, belongs to $(CO)_2$ species. Peak D belongs to a complex between CO and H_2O, and will be referred as a water complex. Like before in the CO/Ar case, Peaks A and B are not susceptible to temperature changes (after heating to 30 K). The dimer peak 2139.9 cm^{-1} is seen most clearly after the annealing cycle at 10 K, and the water complex (2149 cm^{-1} band) gains intensity upon heating from 9 K to 30 K and then remains unchanged.

In the less diluted sample (FA/Ar = 1/150), peaks are seen at the same locations except for the missing water complex 2149 cm^{-1} band. In addition, a broad feature emerges at 2142 cm^{-1}, not observed before in the CO/Ar case. The dimer peak at 2139.9 cm^{-1} is more pronounced relative to Peaks A and B after dissociation at 9 K and after annealing cycle at 10 K. Raising the temperature leaves the peaks at 2138.3 cm^{-1} and 2136.5 cm^{-1} unaltered.

B. Simulated Raman spectra

1. H_2

We start by showing the results where CO is left out from the simulation box. Two different trapping cases were considered, substitution and interstitial site of octahedral symmetry as defined in Table I. In the former site, hydrogen and nearby argon atoms do not move noticeably from their initial perfect lattice positions. In the latter, tighter case, H_2 pushes argons at the corners (in xy-plane) by about 0.26 Å. The rotational potentials are shown for pH_2 in Fig. 4, potentials for oH_2 are nearly identical with minor differences in the last decimals. This is due to different expectation values $\langle 00|\xi^k|00\rangle$ and $\langle 01|\xi^k|01\rangle$ used in the H_2–Ar pair-potential. Rotational and centrifugal constants obtained using the experimental results are $B_0 = 57.89\ cm^{-1}$ and $D_0 = 0.0046\ cm^{-1}$, respectively. These values are used in the numerical simulations.

Crystal field is stronger for the interstitial case, and results in a splitting of the excited state manifold for both para- and orthohydrogen while the ground levels $J = 0$ (A_{1g}) and $J = 1$ (T_{1u}) remain degenerate, respectively. The rotational energies along with the O_h symmetry labels are listed in Table II. The $J = 2$ end state is split into a T_{2g}, E_g -doublet and the $J = 3$ becomes a A_{2u}, T_{2u}, T_{1u} -triplet. The calculated Raman spectra resulting from the potential energy landscape

TABLE II. Rotational manifold energies in cm^{-1} pertaining to rotational transitions in para- and orthohydrogen molecules trapped in substitution (S) and interstitial (O) sites in solid argon. Symmetry labels are in parentheses.

pH_2				
	E_1 (A_{1g})	E_{2-4}(T_{2g})	E_{5-6} (E_g)	
S	0.14	347.3	347.4	
O	7.0	352.2	357.2	
oH_2				
	E_{1-3} (T_{1u})	E_4 (A_{2u})	E_{5-7} (T_{2u})	E_{8-10} (T_{1u})
S	115.9	694.1	694.2	694.2
O	122.8	697.2	700.4	703.1

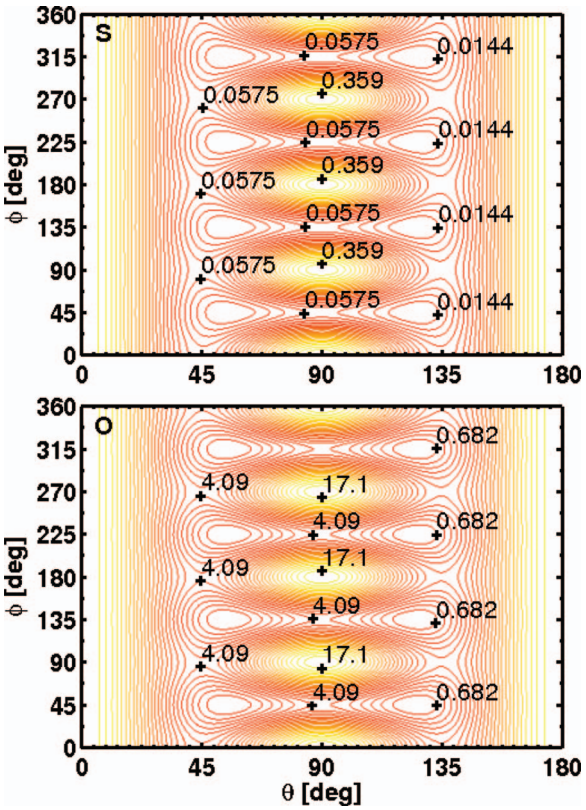

FIG. 4. Rotational energy $V(\theta, \phi)$ in cm^{-1} for the pH_2 in substitution (S) and interstitial (O) sites. Low barrier heights indicate that hydrogen is a nearly free rotor in argon.

is presented in Fig. 5. The S and O sites differ by the single vs. split fine structure pertaining to the energy levels above.

In Fig. 5, we also show the spectra resulting from least-squares fitting of the 10 K experimental spectra to a Lorentzian line shape. The linewidths were parametrized so that they are identical for all transitions originating from the same trapping site. For the pH_2, we chose the width and the intensity as the fit parameters. This resulted in 1.2 cm^{-1} (S) and 4.2 cm^{-1} (O) values for the FWHMs. The ortho case is more difficult to match up to the experimental result. If we allow all the frequencies to change in the fitting procedure, the experimental peak at 572.1 cm^{-1} is not reproduced. Instead the frequencies shift to 575.2 cm^{-1}, 580.0 cm^{-1}, 578.4 cm^{-1} (unchanged), and 584.4 cm^{-1}, and the widths are 1.4 cm^{-1} and 5.1 cm^{-1} for the substitution and interstitial sites, respectively. If we force the first peak to 572.1 cm^{-1}, the line shape is not correctly reproduced. This discrepancy can be removed by introducing different widths for the transitions originating from the interstitial site. Lifting the restraint of identical line widths in the least-squares fitting gives the peaks at 572.1 cm^{-1}, 575.5 cm^{-1}, 578.4 cm^{-1}, and 581.9 cm^{-1}, and their widths are 0.8 cm^{-1}, 2.0 cm^{-1}, 1.5 cm^{-1}, and 5.6 cm^{-1}, respectively. The result is shown in the lower panel of Fig. 5.

When CO is added to the lattice, taking its position at the origin, four cases S1, S2, S3, and O give each a unique signal in the Raman simulations as seen in Fig. 6. The orientation of CO was taken into consideration through Eq. (8). For the S3 case, where the hydrogen is located far away from CO, the

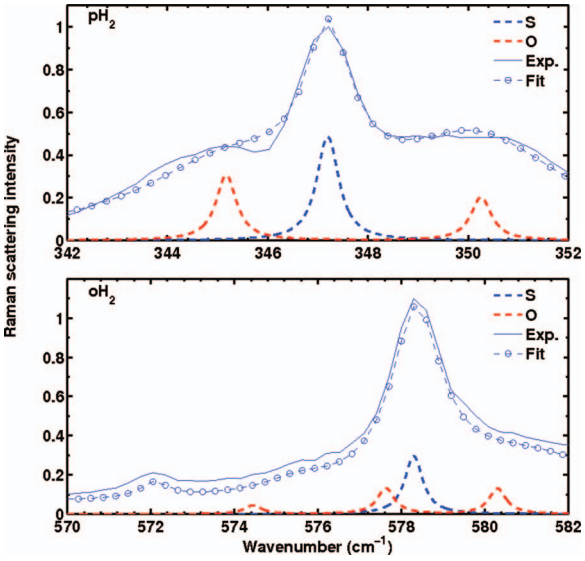

FIG. 5. Simulated rotational Raman spectra for the two H_2 species in Ar. The spectra consist of two calculations, one where the hydrogen is located in the substitution site (S) (broken blue line) and another where the molecule resides in an interstitial site (O) (red broken line). The final observed spectrum is then understood as a sum of the two signals for both hydrogen species (not shown). The experimental spectrum from measurements at 10 K is reproduced for comparison (solid blue line). Also shown is a Lorentzian line shape fit (circles) to the experimental results. See text for the discussion regarding the fit parameters.

Raman shift wavenumbers 347 cm^{-1} and 578 cm^{-1} are identical to those given by the isolated pH_2 and oH_2, respectively, in the substitution site. For the octahedral site (O), the rotational states $J = 2$ and $J = 3$ are again split, but now the splitting is more pronounced due to symmetry breaking induced by the CO. The symmetry states T_{2g} and E_g, responsible for the doublet in the pH_2 case, form mixed states of symmetry and result in the total separation of the $J = 2$ state into five states. With orthohydrogen, the effect is similar ($J = 3$ splits into seven components), but now also the three-fold degeneracy of the ground state ($J = 1$, T_{1u}) is lifted. Further complication arises from the different rotational level structure pertaining to selected CO orientations and is seen as a more complex band structure than one would expect from the degeneracy of the rotational states.

In the S2 configuration, where the molecular hydrogen is a lattice constant away, the spectrum shows a splintered structure where the main peak is approximately on the unperturbed (S) case. The ground state(s) for both types of hydrogen are few wavenumbers higher than in the case of free H_2, the ground state of orthohydrogen being strongly dependent on the orientation of the CO molecule. The excited states $J = 2$ and $J = 3$ show level structures which indicate a triplet and quintet band in the spectrum due to increased crystal-field strength. Like above, the simulated spectra show a structure that is more complex than the above triplet and quintet splitting would indicate and is again due to CO orientations which affect the spectrum via different level structures.

When we consider the case of nearest-neighbors (S1), the rotational energy surface has two equivalent minima ($\theta = 90, \phi = 45, 225$) corresponding to the linear configuration (OC–H–H). The rotational ground state of pH_2 is at

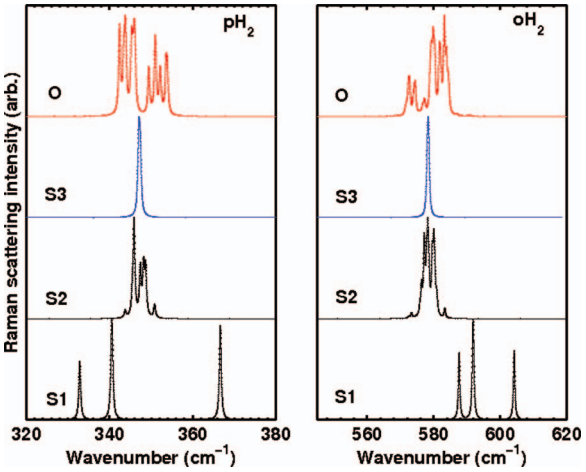

FIG. 6. Simulated rotational Raman spectra for the hydrogens when CO is located at the origin. The H_2 coordinates are marked according to Table I. The individual spectra are normalised.

62 cm^{-1} ($J = 0$, A_{1g}). For the oH_2, the ground state has now become a doublet at 157/194 cm^{-1}. Barrier height for the 180 degree rotation of H_2 in the xy-plane is approximately 90 cm^{-1} for both molecular types. The splitting of the end state of rotational excitation, $J = 2$ and $J = 3$, results now in a triplet and quartet, respectively, such as in S3 but with considerably larger state separation as can be observed in Fig. 6. Here only a single CO orientation is taken into consideration, namely, the OC–H_2 orientation owing to the high barrier for end-over-end rotation of CO molecule (see Fig. 7). The rotational motion is now best described as librational contrary to above cases where the terms hindered rotation and nearly free rotation are best suited.

2. CO

In our previous studies of the pure CO/Ar case, two local lattice configurations were used to explain the Raman and IR spectra. These were referred as SS and DS sites. In the former, argon atoms constitute a perfect fcc lattice around the CO and in the latter a deformation of the perfect lattice is introduced in the form of a vacancy to a nearest-neighbor site. The rotational (and vibrational) motion

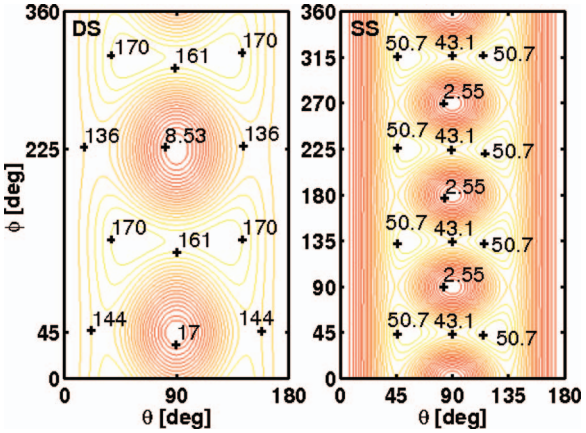

FIG. 7. The adiabatic rotational potential energy surfaces (in cm^{-1}) for isolated CO in DS (left) and SS (right) trapping geometries.

TABLE III. Lowest energy levels (in cm^{-1}) for isolated CO in SS and DS configuration. Row a: adiabatic lattice response is assumed for all CO orientations. Level degeneracies are indicated in parentheses. In the double-substitution site, only OC orientation is reproduced. Rotational constant was 1.24 cm^{-1} and 1.92 cm^{-1} for SS and DS sites, respectively.

Case	E_1	E_2	E_3	E_4	E_5	E_6
			Single-substitution site			
a	24.1	24.9(3)	25.3(2)	43.0(3)	44.9(3)	46.9(3)
			Double-substitution site			
OC–×	39	69	85	99	114	123

in these two cases was found to be very different, in the DS case the molecular axis was seen to oscillate around the direction of vacancy resulting in a librational motion. Two minima were seen in rotational potential, global minimum when the carbon end points toward the vacancy (×), referred as OC orientation (OC$\cdots$ ×), and a local minimum where the molecule was rotated by 180° (CO$\cdots$ ×). The simulations showed a harmonic oscillator-type level structure resulting in a temperature-independent spectra with a single peak at the band origin. In the SS case, we questioned the applicability of the adiabatic model at low temperature limit, and used an approach where the direction of molecular axis is locked due to more static environment. This resulted again in harmonic oscillator-type librational states that gave a temperature independent spectrum. At higher temperatures the notion of adiabatic motion of argon atoms was again introduced, and now the molecule samples the rotational potential that has much lower barriers for rotation. The ground state manifold in this case consisted of three states, the ground state being $J = 0$ (A_{1g}), the next (triple-degenerate) state belonged $J = 1$ (T_{1u}), and the third (double-degenerate) state to $J = 2$ (E_g) in that order with the next manifold of states 20 cm^{-1} higher in energy. The rotational degree of freedom was less confined corresponding to hindered rotation where the motion is a result of quantum tunneling between minima. We have reproduced the adiabatic potentials for SS and DS sites in Fig. 7 and the resulting librational level structure in Table III.

With above information as comparison, we can study the perturbance of H_2 on the rotational motion of CO. Let us first consider the case of S3 and keep in mind that in the hydrogen case, this site gave a signal similar to that originating from the substitution site without CO. The adiabatic surface (see Fig. 8, Panel S3) shows some shifting of the local minima from the isolated case. CO tends to orientate itself approximately along the ⟨100⟩ directions although these are not equivalent anymore. Saddle points at $\theta = 45$, $\phi = 45$ and $\theta = 135$, $\phi = 180$ have now diminished, indicating that hydrogen induces a favorable arrangement of the nearby argon atoms at the positive octant of the crystal frame. Rotational barrier heights between potential wells are higher in energy than in the isolated case, at 50 cm^{-1} and the global maximum is about 63 cm^{-1}.

When hydrogen is in the interstitial site (O), the potential (see Panel O in Fig. 8) is again "skewed" like in the S3 case, but the minima shift to opposite direction and approximately correspond to molecular alignment along the x

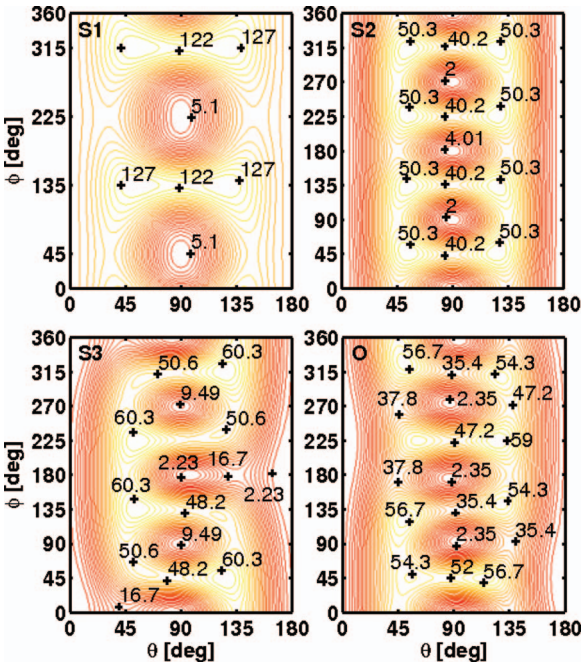

FIG. 8. Fully adiabatic rotational potentials $V(\theta, \phi)$ (in cm^{-1}) for rotating CO in different complex geometries. See text for details.

and y axes. Global maximum is met when C end points toward the triatomic window at ⟨111⟩ direction. There is no single barrier for rotation, rather the value differs when going from rotational well to another on average being over 40 wavenumbers.

In the S2 case, the adiabatic potential surface (Panel S2 in Fig. 8) is seemingly similar to the isolated case, molecular axis pointing toward the x, y, and z axes. However, these orientations do not result in equivalent minima. Global minima correspond to situations where the molecular axis is perpendicular to H_2. We referred to these configurations as T-shaped in Sec. II. Local minima at $\theta = 90, \phi = 0$ and $\theta = 90, \phi = 180$ were called linear configurations, either end of CO pointing toward the hydrogen. Translation takes place along the crystal axes, with T-shape the motion is 0.26 Å along the y and z axes. In the linear configuration, the molecule moves 0.24 Å along the x axis. Initial distance between molecules is $a = 5.31$ Å. When O end points toward the hydrogen, distance is lowered to 5.1 Å, and when CO is rotated in the plane by 180°, the distance increases to 5.5 Å. In a T-shaped configuration, the intermolecular distance sets to 5.29 Å. Hydrogen moves 0.02 Å toward the origin in all orientations. The barrier for rotation is about 40 cm^{-1} and global maxima (52 cm^{-1}) are in the ⟨111⟩ directions.

When hydrogen is as nearest-neighbor in the positive quadrant of xy-plane, the adiabatic potential (Panel S1 in Fig. 8) resembles the situation where the isolated CO resided in the double-substitution cavity. Potential minima belong to CO ($\theta = 90$, $\phi = 45$) and OC ($\theta = 90$, $\phi = 225$) orientations, as either the C or O end can point toward the hydrogen (or vacancy in isolated case). The initial distance is $a/\sqrt{2} = 3.75$ Å and translational motion occurs along the coordinate vector between the molecules such that the center of mass moves 0.4 Å toward the hydrogen in the CO orientation and

TABLE IV. Selected lowest states for adiabatically rotating CO in argon lattice that includes a H_2 molecule in the same unit cell. Rotational constant was $B_0 = 1.92$ cm^{-1} and the values are in wavenumbers. See Table III for rotational levels without the perturbance of hydrogen.

S1							
	E_1	E_2	E_3	E_4	E_5	E_6	E_7
	28.8	49.5	67.0	72.4	88.0	95.2	96.2
S2							
	E_1	E_2	E_3	E_4	E_5	E_6	E_7
	26.8	28.8	28.8	29.9	30.4	32.0	46.9
S3							
	E_1	E_2	E_3	E_4	E_5	E_6	E_7
	24.9	25.2	30.1	30.7	37.5	38.3	45.7
O							
	E_1	E_2	E_3	E_4	E_5	E_6	E_7
	27.2	29.0	29.0	31.1	31.4	31.4	49.1

0.04 Å away in the OC orientation. The intermolecular distance after relaxation is 3.6 Å in the former case and 4.1 Å in the latter. The spherically handled hydrogen molecule has moved 0.02 Å in the x- and y-direction, away from CO, in both orientations.

The rotational Schrödinger equation is solved in above potentials and the resulting energy levels for a selected portion of energy manifold are gathered in Table IV. When hydrogen is farthest away (S3), the symmetry breaking is more profound due to argon atom between the molecules and the six lowest states have mixed contributions from A_{1g}, T_{1u}, E_g, and even from T_{2u} to T_{2g}. The ground state does not belong to $J = 0$ alone anymore but has also a contribution from states with higher quantum number J. The $\Delta n = 1$ transition cannot be identified due to mixing of the next librational manifold with the ground state manifold.

The interstitial site for hydrogen brings the situation again closer to the isolated case, although the state with T_{2g} symmetry has interestingly come down in energy and makes a contribution to the ground state in addition to A_{1g}. Now, the transitions to next manifold ($\Delta n = 1$) are distinguishable from transitions within lowest manifold ($\Delta n = 0$) and are approximately at 18 cm^{-1}.

The similarity of the rotational potential of case S2 with the isolated case is somewhat misleading. In the pair-potential, at the distance of lattice constant, the interaction strength is still noticeable and results in slightly nonequivalent minima in the xy-plane. This nonsymmetry results in a larger splitting of librational levels than in the isolated case. The ground state still belongs to $J = 0$ or A_{1g} symmetry, next two states to $J = 1$ (T_{1u}) like with pure CO, but the next three states show a mixed contribution from $J = 1$ (T_{1u}) and $J = 2$ (E_g) and even from $J = 0$ (A_{1g}) free-rotor states. Transitions to next librational manifold are 16 cm^{-1} above the $\Delta n = 0$ transitions. With hydrogen as a nearest-neighbor (S1), the energy level structure resembles that of a harmonic oscillator and the individual states are superpositions of free-rotor states (up to $J = 4$ for lowest states) such as for the isolated CO in the DS site.

Overall, the effect of a nearby hydrogen seems to have a similar effect on the rotational motion of CO as *vice versa*.

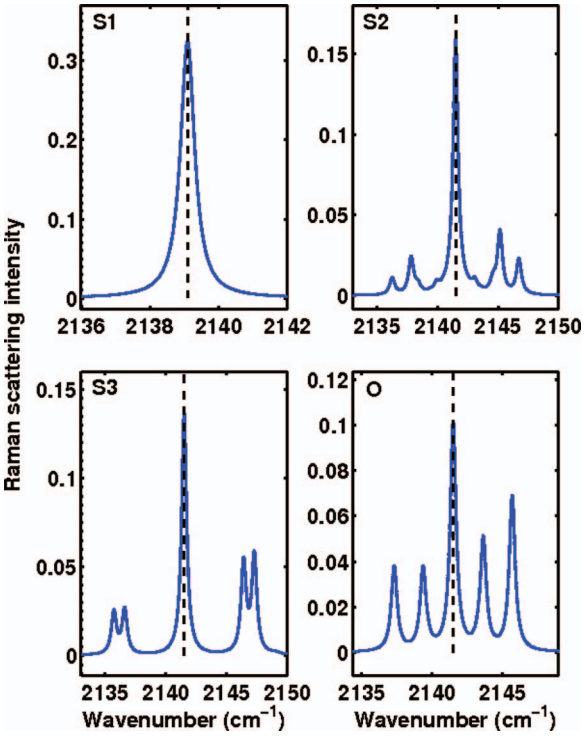

FIG. 9. Simulated rovibrational Raman spectra for complexed CO using potentials shown in Fig. 8. The rotational constant was set to 1.92 cm^{-1}. Transitions to next librational manifold, i.e., the $\Delta n = 1$ transitions, are not shown. Boltzmann distribution corresponds to experiments in 10 K.

This can be attributed to the symmetry breaking of local environment. What matters is not only the distance of hydrogen but the position relative to both CO and nearby argon atoms. This is the reason why the case S2 now gives strikingly similar results to isolated CO: the molecule does not perturb any nearest-neighbor to CO to a great extent. For S3, this is not the case, because one argon is exactly between the molecular species. Our band origin calculations give fundamental frequencies 2139.1 cm^{-1} for OC$\cdots$H$_2$ orientation and 2141.5 cm^{-1} for CO$\cdots$H$_2$. When H_2 is located in the other three sites, we get the same value as in the CO$\cdots$H$_2$ case above. This must be contrasted with our previous results on the isolated case, where we got 2138.7 cm^{-1}, 2140.5 cm^{-1}, and 2141.6 cm^{-1} for OC$\cdots$ $\times$, CO$\cdots$ $\times$, and SS configuration, respectively. The Raman spectra are then simulated with the rotational energy level composition obtained from SE, and using the vibrational frequency from the band origin calculations. The resulting spectra are collected in Fig. 9. Temperature effect via Boltzmann distribution is not included, the rise in temperature would be seen as intensity drop of central feature and broadening of side bands due to larger population at higher states.

IV. DISCUSSION

Rotational and rovibrational spectra of matrix isolated H_2 in argon has been studied in the past by several groups.[36–42] The first recorded spectra were obtained by Prochaska and Andrews[36] who saw two distinct rotational peaks belonging to para- and orthohydrogen at 358 cm^{-1} and 591 cm^{-1},

respectively. Bier *et al.*[37] measured rotational transitions at 351.3 cm^{-1} and 584.2 cm^{-1}. Alikhani *et al.*[39] observed the same transitions at 352.9 cm^{-1} and 584.7 cm^{-1}. Some ten years later, Kornath *et al.*[42] measured rotational transition frequencies at 356.5 cm^{-1} and 587.9 cm^{-1}. To our knowledge, the latter study is the latest Raman measurement on isolated hydrogen in solid argon. The triplet-split structure analogous to that seen in our experiments was first observed by Alikhani *et al.*[39] where the side bands gained intensity as they increased the number of hydrogen molecules in the premixed gas. They only stated that the side peaks are the result of perturbed rotational motion in molecular aggregates. Olbert-Majkut *et al.*[20] measured the rotational Raman transitions of hydrogen molecule after dissociation of formic acid. They saw a singlet structure for oH_2 at 582.1 cm^{-1} and a doublet for pH_2 at 348.6/350.5 cm^{-1}. The explanation for the difference in band splitting was based on the different interactions between CO_2 and para- or orthohydrogen, which was backed by *ab initio* calculations. From our experiments (Fig. 2), with the help of simulations (Fig. 5), the sharp central peaks at frequencies 347.2 cm^{-1} and 578.3 cm^{-1} are assigned to isolated molecular pH_2 and oH_2, respectively, in a single-substitution site. The decrease of 2.5% in the rotational constant from the gas-phase value ($B_0 = 59.326\ cm^{-1}$)[43] indicates a nearly free rotational motion and/or a slight elongation of the bond length. On the other hand, the drastic reduction in the D_0 from the gas-phase value (0.0456 cm^{-1})[43] reflects the stiffness of the molecule in the cage.

The presence of molecular complex CO–H_2 in the matrix is now brought into question. Our numerical results for the fundamental frequency of CO are almost the same as previously without hydrogen.[25] There we had to shift the frequencies by different amounts for DS and SS sites. However, because we do not know the effect of hydrogen on the vibrational motion, shifting the frequencies here would just make the present results to coincide with Peaks A and B of the CO/Ar matrix; therefore, we leave the positions of band origins as a subject of debate. If the hydrogen molecule has only a marginal effect on the vibrational motion of CO, a nearest-neighbor (S1) complex might be hard to distinguish from the DS case (Peak A, see Figs. 3 and 9). The pair-potential for the CO–H_2 complex indicates a strong interaction between fragments and the complexation seems favorable. The initial ballistic trajectory most likely induces the cage exit for the molecular hydrogen, but the thermal diffusion and the van der Waals forces between CO and H_2 might allow the formation of a nearest-neighbor complex in the solid. On the other hand, the high zero-point energy for the H_2 rotating within the matrix-isolated complex might be acting as the separating force between the molecules so that the hydrogen is located where the rotation is less quenched. This is further supported by the comparable energies between the zero-point energy (62 cm^{-1}) and the spherical-averaged intermolecular potential (50 cm^{-1}). The nearest-neighbor complex (S1) must be refused on the basis of the simulated rotational spectrum of hydrogen, where the peaks are separated by tens of wavenumbers (Fig. 6) contrary to the experiment.

If hydrogen is put farther away (S2), the vibrational motion of CO should be the same as in the isolated case, and the central frequency, if shifted, would coincide with Peak B at 2138.3 cm^{-1}. But again, the rich and complex rotational spectrum of H_2 in the simulation does not support the existence of such a nearby-neighbor complex. Turning to S3, where the crystal-field strength is not strong enough to lift the degeneracy of the ground and/or excited rotational state of H_2, the rotational spectrum would consist of single sharp peaks at frequencies identical with the ones for the isolated para/ortho molecule in a substitution site. For CO, this configuration would be observed as a single peak at band origin with shoulders a few wavenumbers equidistant from the central peak. Considering the CO/Ar pseudorotating concept,[34] the lowering of $B_0^{(CO)}$ to 1.24 cm^{-1} would only slightly shift the librational side bands closer to the central peak. This would still give large enough band splitting to make them observable in the spectrum. When H_2 is put into nearest octahedral site (O), the rotational and rovibrational spectrum of H_2 and CO, respectively, show a more profound side band structure in their respective spectra than is observed in the experiments. The possibility that the measured spectra do not originate from configurations O or S2 cannot entirely be ruled out due to line broadening mechanisms that would merge the split-peak structure to a broad band. The spectrum would then be a sum of signals coming from, e.g., S2 and O, giving a qualitatively correct band structure.

Now we return to the H_2/Ar case, and assign, for the first time, the shoulders on the central peak to isolated hydrogen in an octahedral site where the rotation is hindered, and the crystal field induces a splitting of the levels (see Fig. 5). The simulations for pure H_2/Ar mixture with the estimated rotational constant of 57.89 cm^{-1} and the centrifugal constant of 0.0046 cm^{-1}, gave peaks at 345.2 cm^{-1}, 347.2 cm^{-1} (main peak), and 350.2 cm^{-1} for the pH_2, and at 574.4 cm^{-1}, 577.6 cm^{-1}, 578.3 cm^{-1} (main peak), and 580.3 cm^{-1} for the oH_2. The pH_2 peaks coincide with the experimental peaks, but in the oH_2 case, larger splitting is required to match with the experiments. The increase/decrease in intensity of the side bands in annealed matrices are explained as a thermally induced migration of molecular hydrogen to/from interstitial site. Curiously, the appearance of shoulders of the main rotational frequency has not previously been seen in hydrogen doped argon matrices after annealing. This is most likely due to the preferred substitution site when H_2 is co-deposited with Ar. The emergence of side bands as a result of H_2–H_2 dimer formation, as was hypothesized by Alikhani *et al.*,[39] cannot be used as an explanation here because in their experiments a noticeable rise of the side bands occurred at much higher concentration (1:20).

V. CONCLUSIONS

We have measured a Raman signal for the first time from the photoproducts after a dissociation of formaldehyde in solid argon. With the help of simulations, we have assigned the resulting spectra to molecular species CO and H_2. Rovibrational spectrum of CO showed signals from a dimeric species $(CO)_2$ and a CO–H_2O complex along with monomeric species in different lattice geometries (DS and SS sites). A sharp central peak with shoulders on both sides was observed

in the rotational Raman spectrum of ortho- and parahydrogen, which is explained as the crystal-field effect on the rotational motion of isolated hydrogen molecule residing in two different lattice sites, substitution (S) and interstitial (O). Our numerical results show that the existence of nearest-neighbor CO–H_2 complex cannot be responsible for the observed Raman spectra, as the complex should affect the Raman spectrum in the region of both photofragments. The initial cage exit of a translationally hot molecular hydrogen and, most likely, the high zero-point energy of rotational motion of H_2 in thermal equilibrium are the reasons for the separation. The migration of H_2 is not solely responsible for the separation, but we expect the migration of CO to play a role too after the dissociation, which is supported by the observation of bands belonging to a CO–H_2O complex and a CO–CO dimer. The details of the cage exit are unknown, and simulations dedicated to this would help to clarify the apparent non-existence of CO–H_2 intermolecular complex in solid argon. While that kind of simulations are beyond the scope of this work, it would be interesting in future to examine, e.g., by classical trajectories or quantum wavepackets, the fate of the projectile H_2 after the photodissociation event. Regarding the photodissociation event itself, a systematic monitoring of the photofragment production as a function of photon flux along with the absorption spectrum of matrix-isolated FA are required to get information on the branching ratio between molecular and radical pathways.

ACKNOWLEDGMENTS

T.K. and J.L. were supported by the Academy of Finland Decision No. 124974. M.P. and A.O.M. acknowledge the Emil Aaltonen Foundation for funding.

[1]K. Vaskonen, J. Eloranta, T. Kiljunen, and H. Kunttu, J. Chem. Phys. **110**, 2122 (1999).
[2]K. H. Gödderz, N. Schwentner, and M. Chergui, J. Chem. Phys. **105**, 451 (1996).
[3]J. Manz, P. Saalfrank, and B. Schmidt, J. Chem. Soc., Faraday Trans. **93**, 957 (1997).
[4]B. Schmidt, Chem. Phys. Lett. **301**, 207 (1999).
[5]R. B. Gerber, Annu. Rev. Phys. Chem. **55**, 55 (2004).
[6]L. Khriachtchev, M. Pettersson, N. Runeberg, J. Lundell, and M. Räsänen, Nature (London) **406**, 874 (2000).
[7]V. A. Apkarian and N. Schwentner, Chem. Rev. **99**, 1481 (1999).
[8]B. Fu, B. C. Shepler, and J. M. Bowman, J. Am. Chem. Soc. **133**, 7957 (2011).
[9]D. Townsend, S. A. Lahankar, S. K. Lee, S. D. Chambreau, A. G. Suits, X. Zhang, J. Rheinecker, L. Harding, and J. M. Bowman, Science **306**, 1158 (2004).
[10]A. G. Suits, Acc. Chem. Res. **41**, 873 (2008).
[11]A. C. Terentis, S. E. Waugh, G. F. Metha, and S. H. Kable, J. Chem. Phys. **108**, 3187 (1998).
[12]L. R. Valachovic, M. F. Tuchler, M. Dulligan, T. Droz-Georget, and M. Zyrianov, J. Chem. Phys. **112**, 2752 (2000).
[13]J. M. Bowman and X. Zhang, Phys. Chem. Chem. Phys. **8**, 321 (2006).
[14]X. Zhang, J. L. Rheinecker, and J. M. Bowman, J. Chem. Phys. **122**, 114313 (2005).
[15]H. M. Yin, S. H. Kable, X. Zhang, and J. M. Bowman, Science **311**, 1443 (2006).
[16]K. J. Vaskonen and H. M. Kunttu, J. Phys. Chem. A **107**, 5881 (2003).
[17]S. G. Thomas, Jr., and W. A. Guillory, J. Phys. Chem. **77**, 2469 (1973).
[18]J. R. Sodeau and E. K. C. Lee, Chem. Phys. Lett. **57**, 71 (1978).
[19]M. Diem and E. K. C. Lee, Chem. Phys. **41**, 373 (1979).
[20]A. Olbert-Majkut, J. Ahokas, J. Lundell, and M. Pettersson, Phys. Chem. Chem. Phys. **12**, 7138 (2010).
[21]A. Olbert-Majkut, J. Ahokas, J. Lundell, and M. Pettersson, J. Raman Spectrosc. **42**, 1670 (2011).
[22]A. Olbert-Majkut, J. Ahokas, J. Lundell, and M. Pettersson, Chem. Phys. Lett. **468**, 176 (2009).
[23]M. Péalat, D. Debarre, J.-M. Marie, J.-P. E. Taran, A. Tramer, and C. B. Moore, Chem. Phys. Lett. **98**, 299 (1983).
[24]D. Debarre, M. Lefebvre, M. Péalat, J.-P. E. Taran, D. J. Bamford, and C. B. Moore, J. Chem. Phys. **83**, 4476 (1985).
[25]J. Lindgren, A. Olbert-Majkut, M. Pettersson, and T. Kiljunen, Low Temp. Phys. **38**, 708 (2012).
[26]C. B. Moore and J. C. Weisshaar, Annu. Rev. Phys. Chem. **34**, 525 (1983).
[27]D. J. Clouthier and D. A. Ramsay, Annu. Rev. Phys. Chem. **34**, 31 (1983).
[28]P. Jankowski, A. R. W. McKellar, and K. Szalewicz, Science **336**, 1147 (2012).
[29]K. T. Tang and J. P. Toennies, J. Chem. Phys. **118**, 4976 (2003).
[30]C. Bissonnette, C. E. Chuagai, K. G. Crowell, R. J. L. Roy, R. J. Wheatley, and W. J. Meath, J. Chem. Phys. **105**, 2639 (1996).
[31]R. J. L. Roy and H. Wei, University of Waterloo Chemical Physics Report No. CP-659, 2004.
[32]P. Jankowski and K. Szalewicz, J. Chem. Phys. **123**, 104301 (2005).
[33]T. B. Pedersen, J. L. Cacheiro, B. Fernández, and H. Koch, J. Chem. Phys. **117**, 6562 (2002).
[34]J. Manz, J. Am. Chem. Soc. **102**, 1801 (1980).
[35]D. T. Colbert and W. H. Miller, J. Chem. Phys. **96**, 1982 (1992).
[36]F. T. Prochaska and L. Andrews, J. Chem. Phys. **67**, 1139 (1977).
[37]K. D. Bier, H. J. Jodl, and H. Däufer, Can. J. Phys. **66**, 708 (1988).
[38]K. D. Bier, H. J. Jodl, and H. Däufer, Can. J. Phys. **66**, 716 (1988).
[39]M. E. Alikhani, B. Silvi, J. P. Perchard, and V. Chandrasekharan, J. Chem. Phys. **90**, 5221 (1989).
[40]M. E. Alikhani, L. Manceron, J. P. Perchard, and B. Silvi, J. Mol. Struct. **222**, 185 (1990).
[41]M. E. Alikhani, L. Manceron, and J. P. Perchard, J. Chem. Phys. **92**, 22 (1990).
[42]A. Kornath, A. Zoermer, and I. Köper, Spectrochim. Acta, Part A **55**, 2593 (1999).
[43]J. J. Barrett, Appl. Phys. Lett. **29**, 722 (1976).